ISSN 0022-4766, Journal of Structural Chemistry, 2019, Vol. 60, No. 5, pp. 763-771. © Pleiades Publishing, Inc., 2019.
Russian Text © The Author(s), 2019, published in Zhurnal Strukturnoi Khimii, 2019, Vol. 60, No. 5, pp. 796-805.

CATION DISTRIBUTION IN THE COMPOSITE MATERIALS OF THE $CaFe_2O_4$–α-Fe_2O_3 SERIES

Yu. V. Knyazev[1], N. N. Shishkina[2], O. A. Bayukov[1], N. P. Kirik[2], L. A. Solovyov[2], A. M. Zhizhaev[2], E. V. Rabchevsky[2], and A. G. Anshits[2]

Structured composite materials $CaFe_2O_4$–α-Fe_2O_3 (α-Fe_2O_3 content is 2-82 wt.%) are obtained with the method of solid-phase synthesis at 1000 °C. The phase composition of the samples is studied using powder X-ray diffraction. It is shown that the content of $CaFe_2O_4$ and α-Fe_2O_3 phases changes linearly, depending on the composition of the starting material. The scanning electron microscopy data indicate the formation of a two-phase system α-Fe_2O_3–$CaFe_2O_4$. The Mössbauer spectroscopy data at room temperature testify the formation of cationic iron vacancies in the $CaFe_2O_4$ crystal structure in the absence of α-Fe_2O_3 structural defects. Cationic vacancies can be formed during the synthesis in the atmosphere of air.

DOI: 10.1134/S0022476619050081

Keywords: solid-phase synthesis, scanning electron microscopy, Mössbauer spectroscopy, cation vacancies.

INTRODUCTION

In the MO–Fe_2O_3 system, ferrites with the crystal-chemical formula (M)$[Fe]_2O_4$ are usually formed. These materials can be obtained in two crystallographic modifications. If M is a transition metal cation with ionic radius comparable to that of iron, spinel ferrites are formed (cubic crystal cell, space group *Fd*3*m*) [1, 2]. In this case, metal cations appear in tetrahedral and octahedral oxygen environments.

If ionic radius of cations M exceeds 1.0 Å (e.g., Ca, Ba, Sr), the obtained ferrites belong to the orthorhombic crystal family (space group *Pnam*) [3-5]. In such ferrites, iron occupies only octahedral sites, and alkaline earth metal cations are surrounded by oxygens with the coordination number 9. Ferrites with the orthorhombic crystal structure have been studied for a long time [3-7], the most interesting of them is ferrite $CaFe_2O_4$ [8-11]. This is primarily due to the possibility of using this material as a catalyst for the partial oxidation of hydrocarbons and for the production of biofuels [7, 12], in semiconductor devices [13, 14], and in oxygen and ozone gas sensors due to the surface activity of ferrite [15].

In this regard, electronic properties of this ferrite have been widely studied [8-10] and it was shown that calcium ferrite has fairly high resistivity (~10^2-10^3 Ω·cm) and demonstrates *p*-conductivity [9, 16, 17]. Therefore, $CaFe_2O_4$ can be

[1]Kirensky Institute of Physics, Federal Krasnoyarsk Research Center, Siberian Branch, Russian Academy of Sciences, Krasnoyarsk, Russia; yuk@iph.krasn.ru. [2]Institute of Chemistry and Chemical Technology, Federal Krasnoyarsk Research Center, Siberian Branch, Russian Academy of Sciences, Krasnoyarsk, Russia. Original article submitted October 08, 2018; revised November 30, 2018; accepted December 03, 2018.

used in composite materials with oxides such as ZnO and WO_3 to obtain *p–n* junctions [13, 14]. As a result, it was shown that such $CaFe_2O_4$ based composites are highly prospective for the devices of solar energy conversion.

Mössbauer spectroscopy played an important part in the study of $CaFe_2O_4$: it was shown that iron has the charge state 3+ and appears in the octahedral environment of oxygen atoms. The crystal structure of this material formed by FeO_6 octahedra does not contribute to the formation of vacancy states at the atmospheric pressure of oxygen.

In this work, solid-phase synthesis was used to prepare the $CaFe_2O_4$–α-Fe_2O_3 system without the admixtures of foreign phases and to study its phase composition, cationic distribution of iron, and crystal structure defects of the phases as the Fe_2O_3 content in the starting material varies from 74% to 95%.

SAMPLES AND EXPERIMENTAL TECHNIQUES

The following starting reagents were used for the synthesis of $CaFe_2O_4$–α-Fe_2O_3 samples: Fe_2O_3 (*puriss. spec.*, TU 6-09-1418-78) and CaO (*pur.*, GOST 8677-66). The content of Fe_2O_3 in the starting material varied from 74% to 95 wt.%. The reagents were mixed in the required proportions and ground with a KM-1 planetary ball mill for 1 h. The powders were pressed under a pressure of 346 MPa for 1.5-3 min to prepare the pellets with a diameter of 17 mm and a thickness of 1-2 mm. The obtained pellets were annealed at 1000 °C for 4 h and then cooled to room temperature with the oven turned off. The annealed pellets were ground and fractionated using a set of sieves. In the work, the fraction with a particle size of 100-200 μm was used. The samples of this size were chosen in view of their further study as catalytic systems during the oxidative conversion of methane.

Taking into account the difference between the microhardness of CaO and Fe_2O_3, the joint grinding of these oxides is expected to give a matrix composed mainly of Fe_2O_3 particles in the environment of CaO [18]. The subsequent high-temperature synthesis will lead to the formation of the α-Fe_2O_3 composite with a $CaFe_2O_4$ shell. Therefore, there is a perspective of searching novel materials to be used as catalysts, medical magnetic probes, and semiconductor devices.

The chosen method of synthesis allows obtaining samples within a wide range of chemical and phase compositions and to create core–shell systems with the core formed by Fe_2O_3 which demonstrates higher microhardness [19]. The composition of the initial materials was chosen with the account of phase equilibrium data for the CaO–Fe_2O_3 system in air [20].

The quantitative phase composition of the samples, microstructural characteristics of the phases were determined by powder XRD using the Rietveld full-profile refinement and the method of derivative difference minimization (DDM) on a powder X-ray diffractometer X′Pert Pro MPD (PANalytical, Netherlands) equipped with a solid-state detector PIXcel and a secondary graphite monochromator (CoK_α-radiation) similar to [21].

The composition, surface structure of the particles and their polished cuts were studied using a scanning electron microscope (SEM) *TM*-3000 (Hitachi, Japan) with a Quantax70 microanalysis system equipped with a Bruker XFlash 430H energy-dispersive X-ray spectrometer (EDS) (Germany). The acquisition time was determined from the quality of the spectrum assembly required for the quantitative processing and exceeded 10 min.

The Mössbauer spectra were obtained on a MS-1104Em spectrometer (Research Institute of Physics of the Southern Federal University) at room temperature in transmission geometry with a ^{57}Co(Cr) radioactive source. The spectra were interpreted in two stages. At the first stage, possible non-equivalent sites of iron in the samples were determined by calculating the probability distribution of quadrupole splittings and hyperfine fields. The obtained results were used to construct a preliminary model of the spectrum. At the next stage, the model spectra were fitted to experimental spectra by varying the entire set of hyperfine parameters using linear least squares approximations.

RESULTS

Powder X-ray analysis. As an example, Fig. 1 shows an XRD pattern for the sample 85 obtained from the starting materials composed of 85% Fe_2O_3 and 15% CaO. According to the XRD difference spectrum (Fig. 1), the sample contains

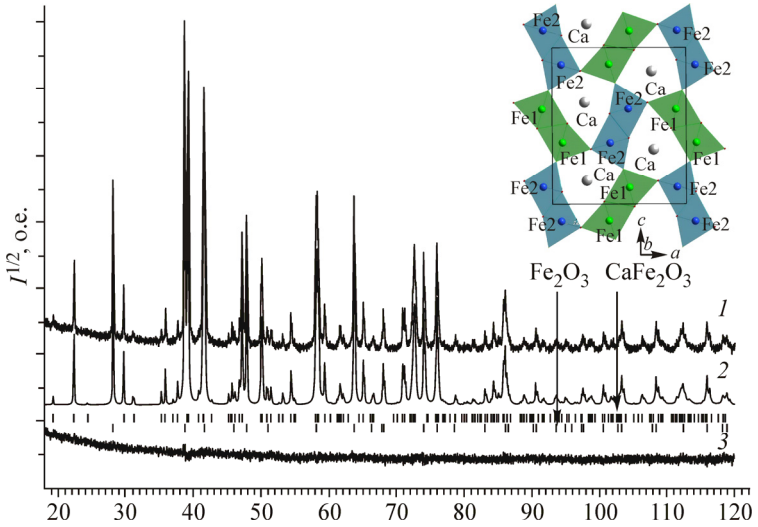

Fig. 1. XRD patterns of the 85% Fe_2O_3 sample: experimental (*1*), calculated after the DDM refinement (*2*), difference curve (*3*). The inset shows the $CaFe_2O_4$ crystal structure.

TABLE 1. Phase Composition of the Samples Depending on the Fe_2O_3 Content in the Starting Materials

Sample	Composition of starting materials, Fe_2O_3/CaO, wt.%	Phase content, wt.%	
		$CaFe_2O_4$	α-Fe_2O_3
74	74 / 26	98	2
78	77.7 / 22.3	81	19
80	80 / 20	73	27
85	85 / 15	55	45
90	90 / 10	33	67
95	95 / 5	18	82

two crystallographic phases $CaFe_2O_4$ and α-Fe_2O_3 with the contents of 55% and 45%, respectively. Table 1 shows the XRD data for all samples. All studied samples are two-phase systems composed of ferrites $CaFe_2O_4$ and α-Fe_2O_3. As can be seen, the starting material with the composition of 74% Fe_2O_3 and 26% CaO gives almost pure ferrite $CaFe_2O_4$ with a 2% admixture of α-Fe_2O_3. These data agree with the phase diagram of the CaO–Fe_2O_3 system [20]. As the relative content of iron oxide in the starting material increases, a two-phase system $CaFe_2O_4$–α-Fe_2O_3 is formed. The highest hematite content is achieved in the sample 95 (16% $CaFe_2O_4$ and 82% α-Fe_2O_3).

The unit cell parameters of $CaFe_2O_4$ correspond to previously reported data [4, 9, 10]. The structure of this ferrite was studied in detail in the works [4, 9] where the main features of $CaFe_2O_4$ were established. This ferrite has two non-equivalent iron sites with the octahedral coordination of oxygen (Fe1, Fe2). The oxygen octahedra demonstrate different degrees of distortion in these sites, so that the distortions in the Fe1 site are stronger than those in the Fe2 site [9, 10].

Fig. 2 shows unit cell parameters of $CaFe_2O_4$ as functions of the α-Fe_2O_3 content in the samples. Parameter *c* decreases and parameter *b* slightly increases as the hematite content in the samples increases. In this case, the hematite unit cell parameters can be considered constant. Such a small change in the unit cell parameters indicates the stability of the phases in the samples.

SEM–EDS analysis. The SEM–EDS studies were performed on the polished cuts for the whole series of the samples. As an example, Fig. 3 shows SEM images of samples 74 and 90. The black spots in the micrographs (left side of Fig. 3) are the pores formed in the samples during the synthesis. Darker and lighter areas in the elemental mapping (right side of Fig. 3) correspond to Fe and Ca cations, respectively.

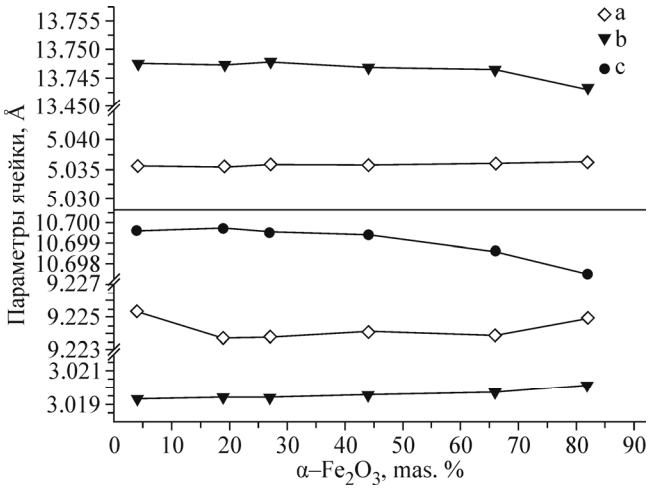

Fig. 2. Crystal cell parameters in α-Fe_2O_3 (top) and $CaFe_2O_4$ (bottom) samples depending on the content of the α-Fe_2O_3 phase in the samples.

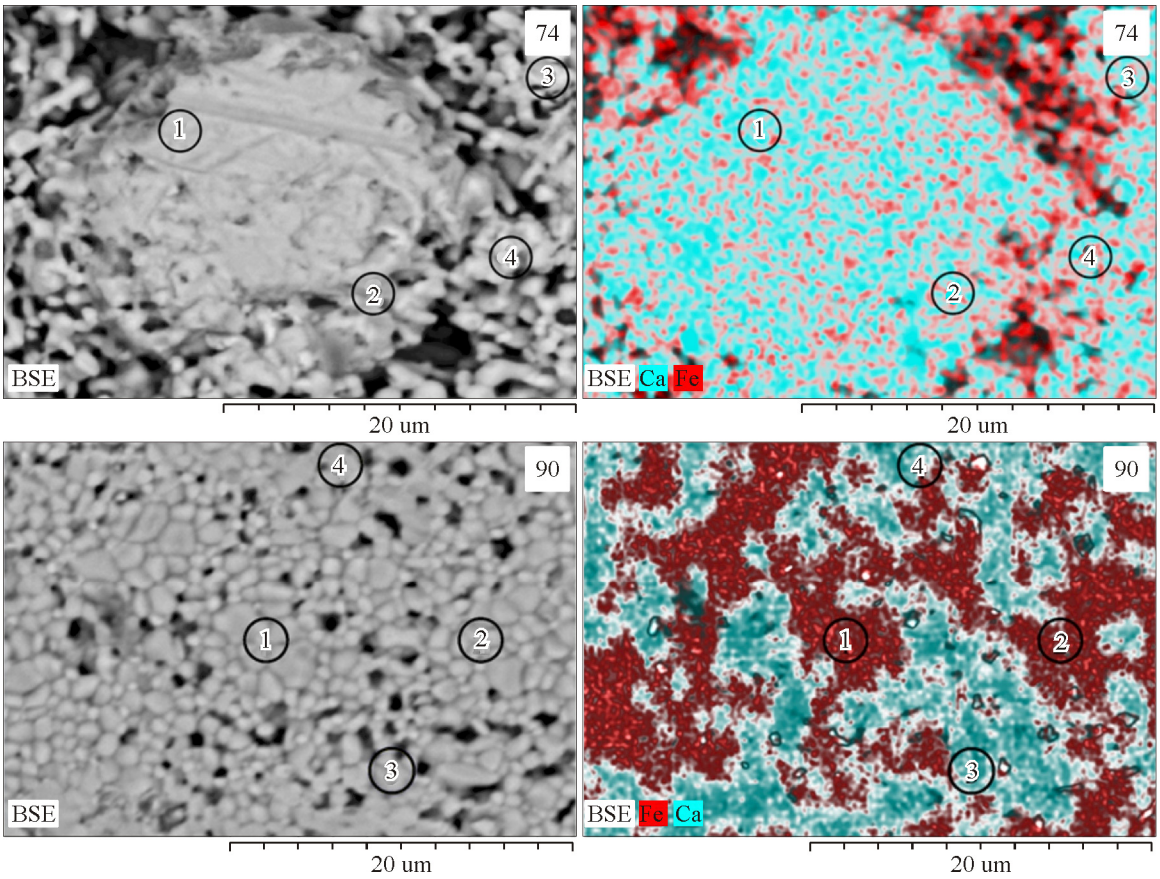

Fig. 3. SEM images with local areas of elemental analysis (left) and elemental mapping images (right); light areas correspond to Ca, dark areas correspond to Fe.

The samples exhibit porous inhomogeneous structures which are changed as the content of iron oxide increases. In the sample 74 (the α-Fe_2O_3 content is 2 wt.%, according to powder XRD data), the SEM–EDS analysis testifies almost uniform distribution of Fe and Ca cations over the sample cut, the grains of the $CaFe_2O_4$ phase are about 10-25 μm in size. As the content of α-Fe_2O_3 increases, individual areas are formed, which is clearly seen in the elemental mapping. These areas are

composed of the hematite phase in the $CaFe_2O_4$ matrix and increase in size as the content of α-Fe_2O_3 in the samples increases. For example, sample 90 (α-Fe_2O_3 content is 67 wt.%) contains dense 0.5-4 μm grains of the α-Fe_2O_3 phase surrounded by a "framework" of a less dense $CaFe_2O_4$ phase.

Table 2 shows the analysis of local areas ($d \approx$ 3-6 μm) on the surfaces of the samples with respect to chemical elements. In sample 74, all studied areas have close compositions, which are in good agreement with the composition of calcium ferrite $CaFe_2O_4$ (73.68 wt.% Fe and 26.32 wt.% Ca). As the hematite content increases, the dense areas of the samples (areas 1 and 2) become enriched with Fe and depleted with Ca as compared to their initial content.

Mössbauer spectroscopy. Fig. 4 shows the Mössbauer spectra of the samples. The experimental spectra recorded at

TABLE 2. Elemental Analysis Data Obtained for the Local Areas of Polished Cuts of Samples 74 and 90

Sample	Content of chemical elements, wt.%			
	Areas 1 and 2		Areas 3 and 4	
	Fe	Ca	Fe	Ca
74	70.6-73.6	26.4-29.4	71.6-72.6	27.4-28.4
90	96.9-99.0	1.0-3.1	73.6-78.7	21.3-26.4

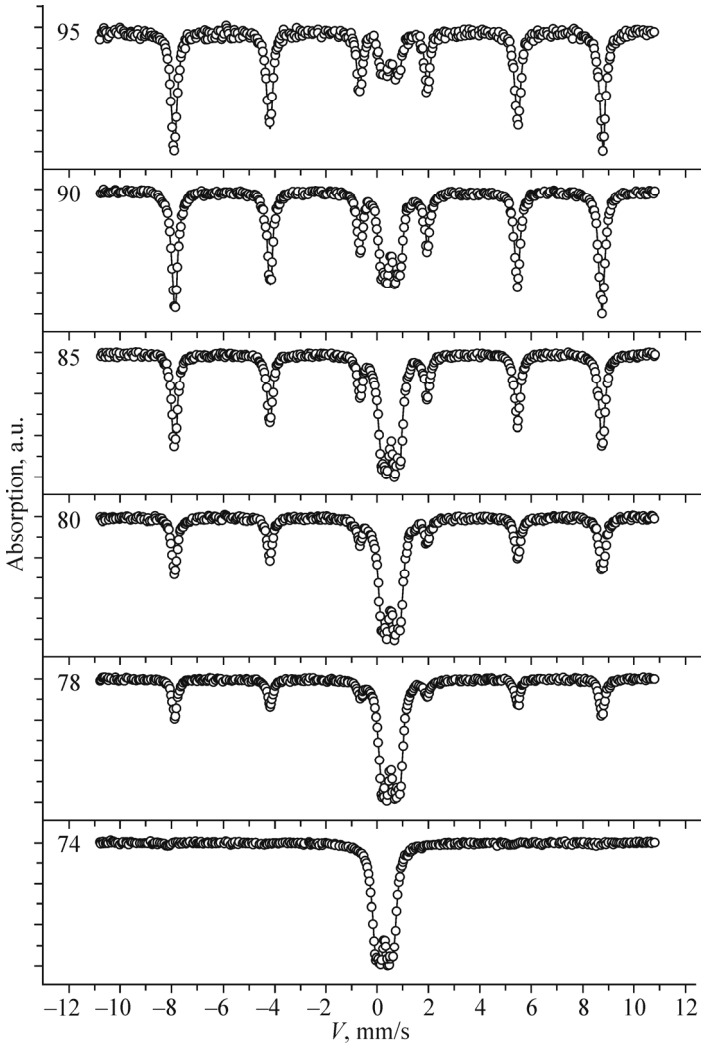

Fig. 4. Mössbauer spectra of the samples recorded at 300 K. Symbols show the experimental spectra, solid lines show the results of spectra processing.

room temperature confirm the powder XRD data as far as the presence of a two-phase system. The spectra are the sums of Zeeman sextets and paramagnetic doublets. The figure clearly shows the change in the intensities of the sextet lines and the paramagnetic part of the spectra to indicate that the ratio of the phase composition in the $CaFe_2O_4$–α-Fe_2O_3 system varies largely together with the changes in the content of Fe_2O_3–CaO oxides in the starting materials.

The Mössbauer parameters of the spectra are shown in Table. 3. The penultimate column shows the atomic content of iron in the corresponding crystallographic phase and in the nonequivalent site for $CaFe_2O_4$. The paramagnetic part of the spectra consists of two quadrupole doublets that belong to the $CaFe_2O_4$ phase [10, 22], and the magnetic sextet corresponds to α-Fe_2O_3 [23]. The phase ratio in the samples is very sensitive to the composition of the starting materials, which is indicated by its wide variation for the initial Fe_2O_3 content of 74-95 wt.%. in the starting material

The magnitudes of chemical shifts and quadrupole splittings indicate that iron cations in $CaFe_2O_4$ are in a high-spin state and their charge state is 3+ [24, 25]. These cations occupy two crystallographic octahedral sites which have nonequivalent distortion degrees of the local environment.

RESULTS AND DISCUSSION

According to the phase diagram [18] and powder XRD data, the excess content of Fe_2O_3 in the starting materials leads to the formation of a highly porous two-phase system $CaFe_2O_4$–α-Fe_2O_3. Note that only very low-porous samples of stoichiometric composition $CaFe_2O_4$ were previously studied [9]. The electron microscopy and EDS data obtained for the samples of the CaO–Fe_2O_3 oxide system suggest that the samples have a fragmentary core–shell structure, where the core is formed by hematite and the shell is formed by the calcium ferrite phase $CaFe_2O_4$.

TABLE 3. Mössbauer Parameters of CaO–Fe_2O_3 Samples

Sample	*IS*, ±0.005 mm/s	*H*, ±5 kOe	*QS*, ±0.01 mm/s	*W*, ±0.01 mm/s	*A*, ±0.03 at.%	Position/Phase
74	0.383	517	–0.44	0.32	0.04	α-Fe_2O_3
	0.371	–	0.72	0.28	0.52	Fe1–$CaFe_2O_4$
	0.369	–	0.29	0.26	0.45	Fe2–$CaFe_2O_4$
78	0.383	517	–0.41	0.21	0.30	α-Fe_2O_3
	0.379	–	0.73	0.26	0.37	Fe1–$CaFe_2O_4$
	0.376	–	0.29	0.26	0.33	Fe2–$CaFe_2O_4$
80	0.382	517	–0.43	0.24	0.41	α-Fe_2O_3
	0.376	–	0.73	0.30	0.31	Fe1–$CaFe_2O_4$
	0.375	–	0.29	0.26	0.28	Fe2–$CaFe_2O_4$
85	0.381	517	–0.41	0.24	0.56	α-Fe_2O_3
	0.379	–	0.74	0.26	0.23	Fe1–$CaFe_2O_4$
	0.376	–	0.30	0.26	0.21	Fe2–$CaFe_2O_4$
90	0.380	516	–0.41	0.25	0.69	α-Fe_2O_3
	0.373	–	0.74	0.26	0.16	Fe1–$CaFe_2O_4$
	0.372	–	0.31	0.24	0.15	Fe2–$CaFe_2O_4$
95	0.383	518	–0.41	0.25	0.82	α-Fe_2O_3
	0.366	–	0.72	0.26	0.09	Fe1–$CaFe_2O_4$
	0.359	–	0.30	0.24	0.09	Fe2–$CaFe_2O_4$

Chemical isomeric shift with respect to α-Fe (*IS*); quadrupole splitting (*QS*); Mössbauer line width at half height (*W*); relative site occupancy (*A*).

According to the above powder XRD and Mössbauer spectroscopy data, the ratio of $CaFe_2O_4$ and the α-Fe_2O_3 phase in the samples is highly dependent on the composition of the starting material. The content of hematite in the samples increases together with the content of Fe_2O_3 in the starting material and reaches its maximum value of 82% in the sample 95. Fig. 5 juxtaposes the phase composition (in wt.%) of the samples obtained with powder XRD and Mössbauer spectroscopy methods. Mössbauer spectroscopy is very sensitive to the presence of various iron-containing phases which can be formed from these starting materials under certain conditions [10, 26]. The phase composition of the samples estimated using Mössbauer spectroscopy is in qualitative agreement with the XRD data, and the phase content changes almost linearly with respect to the Fe_2O_3 content in the starting materials.

The distortion of the local environment around the Mössbauer cation is characterized by the quadrupole splitting of the paramagnetic doublet; therefore, the formation of additional phases at the boundary between $CaFe_2O_4$ and α-Fe_2O_3 is to be associated with a sharp increase of local distortion (and, consequently, *QS*). In our case, the change of *QS* for $CaFe_2O_4$ (Fig. 6) for each non-equivalent Fe site virtually does not exceed the experimental error. Thus, the increased content of α-Fe_2O_3 does increase local distortions and indicates the absence of additional transition phases between $CaFe_2O_4$ and α-Fe_2O_3

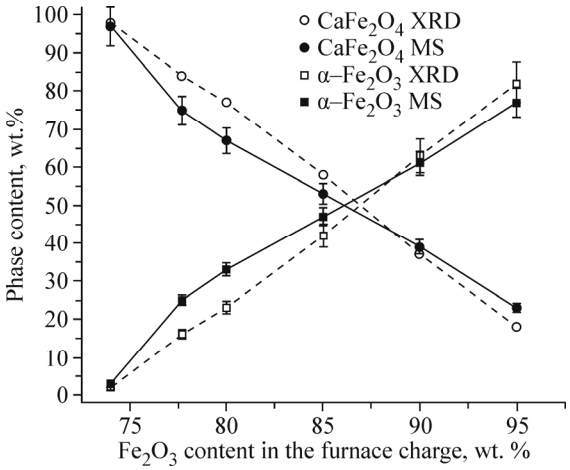

Fig. 5. Phase content of CaO–Fe_2O_3 samples prepared at 1000 °C, depending on the Fe_2O_3 content in the starting materials. The experimental error is shown.

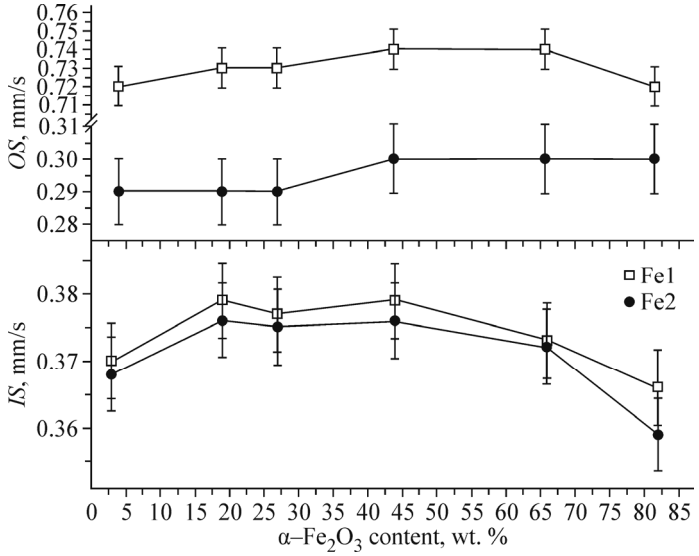

Fig. 6. Quadrupole splitting *QS* and isomeric shift *IS* in $CaFe_2O_4$ samples plotted as functions of α-Fe_2O_3 content.

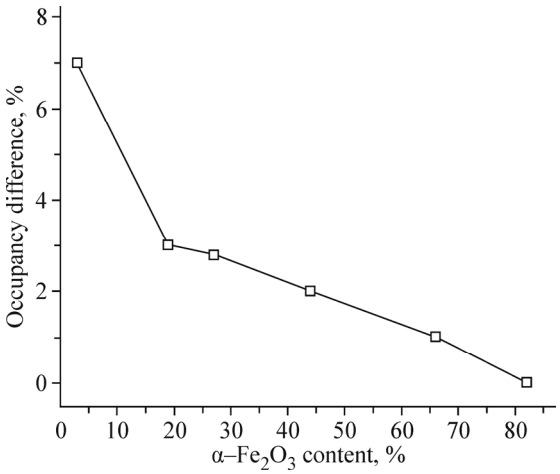

Fig. 7. Occupancy difference between nonequivalent sites of Fe cations in $CaFe_2O_4$ as a function of α-Fe_2O_3 content in the samples.

phases in the samples. The Mössbauer spectroscopy data [9] indicate that the number of anion vacancies in $CaFe_2O_4$ (and, consequently, the nonstoichiometry of the composition) is very small and does not affect the charge state of iron cations, which can be estimated by the magnitude of the chemical shift (*IS*). Since the magnitude of the chemical shift in the studied samples depends but slightly on the phase content, it can be concluded that no anion oxygen vacancies are present in our case (Fig. 6). That is, the change in the occupancy of nonequivalent sites (Table 3) is not associated with the defects in the ferrite crystal structure, which remains close to that of pure samples [4, 9, 10] in spite of the presence of α-Fe_2O_3.

The fact that the occupancy of nonequivalent sites Fe1 and Fe2 in the ferrite $CaFe_2O_4$ depends on the α-Fe_2O_3 content (Table 3) indicates the appearance of cationic vacancies in the $CaFe_2O_4$ structure in the crystallographic site Fe2. The content of vacancies as a function of hematite content is shown in Fig. 7. The defectiveness of ferrite was previously detected in Mössbauer spectra [10] when studying $CaFe_2O_4$ samples prepared at 900 °C under different partial pressures of oxygen in atmosphere. It was shown that cationic vacancies in the sample appear only when the oxygen partial pressure decreases below 10^{-10} atm., i.e. the presence of the vacancies is due to the loss of most chemically active oxygen atoms in the lattice.

In our case, cationic vacancies are formed during the synthesis in air; moreover, it was found that the largest number of vacancies is observed for sample 74, which is the closest to the samples studied in [9, 10]. The increase in α-Fe_2O_3 content causes a monotonous decrease in the number of vacancies and the stabilization of the stoichiometry of the $CaFe_2O_4$ ferrite structure. As shown above, the samples are a core–shell system where the core is formed by α-Fe_2O_3. Since the maximal occupancy difference between nonequivalent sites of iron in $CaFe_2O_4$ is achieved for the α-Fe_2O_3 content of 2% in the sample, it can be concluded that the ferrite structure $CaFe_2O_4$ is stabilized by the α-Fe_2O_3 core. Thus, the variation of the Fe_2O_3 content in the starting material can be used to control the distribution of iron cations in the $CaFe_2O_4$ structure over nonequivalent crystallographic positions Fe1 and Fe2.

CONCLUSIONS

Two-phase samples $CaFe_2O_4$–α-Fe_2O_3 with the content of α-Fe_2O_3 equal to 2-82 wt.% were prepared at 1000 °C from a mixture of oxides CaO–Fe_2O_3 using the method of solid-phase synthesis. No other phases were detected with the powder X-ray analysis. The Mössbauer spectroscopy data indicate the defectiveness of the $CaFe_2O_4$ structure caused by cationic iron vacancies in the nonequivalent crystallographic sites Fe2. According to SEM–EDS data, excess content of Fe_2O_3 (relative to the stoichiometric starting material $CaFe_2O_4$) leads to the formation of fragmentary core–shell samples where α-Fe_2O_3 forms the core and stabilizes the $CaFe_2O_4$ ferrite structure by reducing the number of cationic vacancies. Such effect

of α-Fe_2O_3 on the cationic distribution can be used to control the cationic distribution of iron in $CaFe_2O_4$. The reasons that cationic vacancies appear in the $CaFe_2O_4$ crystal structure and their effect on the physicochemical properties of ferrite require further research.

FUNDING

The study was performed with the financial support of the Russian Foundation for Basic Research, the Government of the Krasnoyarsk Krai, the Krasnoyarsk Regional Science Foundation within the project No. 18-42-243011 “The effect of the composition and the defective structure of $CaFe_2O_4$ based “core–shell” composite materials on their electronic and catalytic properties” and the UMNIK program.

CONFLICT OF INTERESTS

The authors declare that they have no conflict of interests.

REFERENCES

1. W. H. Bragg. *The London, Edinburgh, and Dublin Philos. Mag. J. Sci.*, **1915**, *30*, 305.
2. D. Guin, B. Baruwati, and S. V. Manorama. *J. Mol. Catal. A: Chem.*, **2005**, *242*, 26.
3. F. P. Glasser and L. D. Glasser. *J. Am. Ceram. Soc.*, **1963**, *46*, 377.
4. B. F. Decker and J. S. Kasper. *Acta Crystallogr.*, **1957**, *10*, 332.
5. C. Do-Dinh, E. F. Bertaut, and J. Chappert. *J. Phys. (Paris)*, **1969**, *30*, 566
6. H. Yamamoto, T. Okada, H. Watanabe et al. *J. Phys. Soc. Jpn*, **1968**, *24*, 275.
7. D. Hirabayashi, T. Yoshikawa, Y. Kawamoto et al. *Adv. Sci. Technol. (Durnten-Zurich, Switz.)*, **2006**, *45*, 2169.
8. K. Obata, Y. Obukuro, S. Matsushima et al. *J. Ceram. Soc. Jpn.*, **2013**, *121*, 766.
9. E. V. Tsipis, Y. V. Pivak, J. C. Waerenborgh et al. *Solid State Ionics*, **2007**, *178*, 1428.
10. V. V. Kharton, E. V. Tsipis, V. A. Kolotygin et al. *J. Electrochem. Soc.*, **2008**, *155*, 13.
11. B. F. Decker and J. S. Kasper. *Acta Crystallogr.*, **1957**, *10*(4), 332.
12. Bao-jin Xue, J. Luo, and F. Zhang. *Energy*, **2014**, *68*, 584.
13. C. Shifu, Z. Wei, L. Wei et al. *Chem. Eng. J.*, **2009**, *155*, b466.
14. R. Wan, C. Jia, and W. Zhang. *J. Alloys Compd.*, **2012**, *544*, 1.
15. Y. Matsumoto, F. Nitta, J. Hombo et al. *J. Electrochem. Soc.*, **1991**, *138*, 1701.
16. Y. Matsumoto, J. Hombo, and F. Nitta. *J. Appl. Phys*., **1989**, *66*, 5109.
17. Y. Matsumoto, M. Obata, and J. Hombo. *J. Phys. Chem.*, **1994**, *98*, 2950.
18. G. V. Samsonov. Physical and Mechanical Properties of Oxides. Handbook [in Russian]. Metallurgy: Moscow, **1978**.
19. Reactions in the Solid State. / Eds. M. Brown, D. Dollimore, A. Knox Galwey. Vol. 22. Elsevier: Amsterdam, **1980**, 340.
20. B. Phillips and A. Muan. *J. Am. Ceram. Soc*., **1958**, *41*, 445.
21. O. M. Sharonova, N. N. Anshits, L. A. Solovyov et al. *Fuel*, **2013**, *111*, 332.
22. A. Hudson and H. J. Whitfield. *J. Chem. Soc. (A)*, **1967**, 376.
23. R. E. Vandenberghe, A. E. Verbeeck, E. De Grave et al. *Hyperfine Interact.*, **1986**, *29*, 1157.
24. C. A. McCammon, A. I. Becerro, F. Langenhorst et al. *J. Phys.: Condens. Matter*, **2000**, *12*, 2969.
25. J. C. Waerenborgh, D. P. Rojas, A. L. Shaula et al. *Mater. Lett.*, **2004**, *58*, 3432.
26. D. Hirabayashi, Y. Sakai, T. Yoshikawa et al. *Hyperfine Interact.*, **2006**, *167*, 809.